

## Experimental and Monte Carlo dosimetric characterization of a 1 cm $^{103}\text{Pd}$ brachytherapy source

Joshua L. Reed<sup>1,\*</sup>, Mark J. Rivard<sup>2</sup>, John A. Micka<sup>1</sup>, Wesley S. Culberson<sup>1</sup>, Larry A. DeWerd<sup>1</sup>

<sup>1</sup>Department of Medical Physics, University of Wisconsin–Madison, UW Medical Radiation Research Center, Madison, WI

<sup>2</sup>Department of Radiation Oncology, Tufts University School of Medicine, Boston, MA

### ABSTRACT

**PURPOSE:** To determine the in-air azimuthal anisotropy and in-water dose distribution for the 1 cm length of a new elongated  $^{103}\text{Pd}$  brachytherapy source through both experimental measurements and Monte Carlo (MC) simulations. Measured and MC-calculated dose distributions were used to determine the American Association of Physicists in Medicine Task Group No. 43 (TG-43) dosimetry parameters for this source.

**METHODS AND MATERIALS:** The in-air azimuthal anisotropy of the source was measured with a NaI scintillation detector and was simulated with the MCNP5 radiation transport code. Measured and MC results were normalized to their respective mean values and then compared. The source dose distribution was determined from measurements with LiF:Mg,Ti thermoluminescent dosimeter (TLD) microcubes and MC simulations. TG-43 dosimetry parameters for the source, including the dose-rate constant,  $A$ , two-dimensional anisotropy function,  $F(r, \theta)$ , and line-source radial dose function,  $g_L(r)$ , were determined from the TLD measurements and MC simulations.

**RESULTS:** NaI scintillation detector measurements and MC simulations of the in-air azimuthal anisotropy of the source showed that  $\geq 95\%$  of the normalized values for each source were within 1.2% of the mean value. TLD measurements and MC simulations of  $A$ ,  $F(r, \theta)$ , and  $g_L(r)$  agreed to within the associated uncertainties.

**CONCLUSIONS:** This new  $^{103}\text{Pd}$  source exhibits a high level of azimuthal symmetry as indicated by the measured and MC-calculated results for the in-air azimuthal anisotropy. TG-43 dosimetry parameters for the source were determined through TLD measurements and MC simulations.

© 2014 American Brachytherapy Society. Published by Elsevier Inc. All rights reserved.

### Keywords:

CivaString; CS10; Brachytherapy;  $^{103}\text{Pd}$ ; Dosimetry characterization

### Introduction

Permanent prostate brachytherapy has commonly been performed with titanium-encapsulated  $^{125}\text{I}$  or  $^{103}\text{Pd}$  sources with overall lengths on the order of 0.5 cm (1–3). Many of these sources contain internal components that are free to

move and occupy a variety of positions, resulting in increased uncertainty in the dose distribution around the source because of uncertainties in the positioning of the radioactive material and high-Z internal components (4). The CivaString  $^{103}\text{Pd}$  brachytherapy source from CivaTech Oncology, Inc. (Research Triangle Park, NC) is a new elongated brachytherapy source made of a low-Z organic polymer that provides stable internal and external geometries. This source is available in 1 cm integer lengths ranging from 1 to 6 cm. The focus of this study is the dosimetric characterization of the 1 cm source, referred to here as the CS10, through both experimental measurements using thermoluminescent dosimeters (TLDs) and Monte Carlo (MC) simulations with the MCNP5 radiation transport code (Los Alamos National Laboratory, Los Alamos, NM) in accordance with the American Association of Physicists in Medicine Task Group No. 43 Report (TG-43) (2). The

Received 11 November 2013; received in revised form 6 March 2014; accepted 8 April 2014.

Financial disclosure/Conflict of interest: JLR, JAM, WSC, and LAD received partial support from an educational grant from CivaTech Oncology, Inc. MJR received research support from CivaTech Oncology, Inc.

The results of this work were presented in part at the American Brachytherapy Society 2013 Annual Meeting in New Orleans, LA.

\* Corresponding author. Department of Medical Physics, University of Wisconsin–Madison, UW Medical Radiation Research Center, 1111 Highland Avenue, B1002 WIMR, Madison, WI 53705-2275. Tel.: +1-608-262-6320; fax: +1-608-262-5012.

E-mail address: jreed2@wisc.edu (J.L. Reed).

present investigation complements the investigation by Rivard *et al.* (5) that involved MC assessment of the CivaString source.

In this article, certain commercially available products are referred to by name. These references are for informational purposes only and imply neither endorsement by the University of Wisconsin Medical Radiation Research Center (UWMRRC) nor that these products are the best or only products available for the purpose.

## Methods and materials

### Source description

Details of the dimensions, material compositions, material densities, and distribution of radioactive  $^{103}\text{Pd}$  material within the CS10 source were obtained from CivaTech Oncology, Inc. The CS10 source consists of a gold marker, four regions that each contain  $^{103}\text{Pd}$ , and a low-Z organic polymer. The gold marker and  $^{103}\text{Pd}$  regions occupy fixed positions within the source. A schematic diagram of the source is shown in Fig. 1.

The gold marker is a cylindrical rod with a diameter of 0.025 cm and a length of 0.080 cm and is centered along the length of the source with its cylindrical axis parallel to the longitudinal axis of the source. There is a nominal 0.0055 cm distance between the central cylindrical axis of the gold marker and the central cylindrical axis of the organic polymer. Two  $^{103}\text{Pd}$  regions are located on either side of the gold marker. Each of the four  $^{103}\text{Pd}$  regions is shaped like an elongated isosceles trapezoidal prism with a long base with a length of 0.210 cm, a short base with a length of 0.194 cm, a height of 0.025 cm, and a width of 0.028 cm. With the origin defined at the source center, the centers of the four  $^{103}\text{Pd}$  regions are positioned at longitudinal distances of  $-0.389$ ,  $-0.167$ ,  $0.167$  cm, and  $0.389$  cm, with the  $^{103}\text{Pd}$  material spanning a distance of 0.988 cm. There is a nominal 0.0035 cm distance between the center of the  $^{103}\text{Pd}$  regions and the central cylindrical axis of the organic polymer. The gold marker and  $^{103}\text{Pd}$  regions are fixed in a cylindrical organic polymer material that was simulated as having a length of 1.09 cm and an outer diameter of 0.085 cm. The length and outer diameter of the cylindrical organic polymer material of three CS10

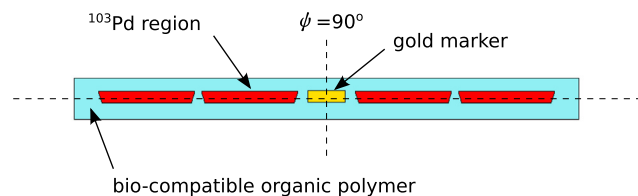


Fig. 1. Schematic diagram of the CivaString CS10 source. The gold marker is shown in yellow, the  $^{103}\text{Pd}$  regions are shown in red, and the low-Z organic polymer material is shown in light blue.  $\psi$  indicates the azimuthal angle for the MC model of the CS10 source. MC = Monte Carlo.

sources were measured with digital calipers. The measured lengths were within 0.03 cm of the simulated value of 1.09 cm, and the measured outer diameters were within 0.008 cm of the simulated value of 0.085 cm. The organic polymer material has a mass density of  $1.15 \text{ g/cm}^3$ , and its weight fractions are  $\text{H} = 0.085$ ,  $\text{C} = 0.648$ ,  $\text{N} = 0.050$ , and  $\text{O} = 0.217$  (courtesy of CivaTech Oncology, Inc.).

For the purpose of calculating TG-43 dosimetry parameters, the active length of the source is assumed to be 1.0 cm. This active length represents an approximate model of the spatial distribution of radioactive material within the CS10 source, being only 0.012 cm greater than the distance spanned by the  $^{103}\text{Pd}$  material. Use of this active length value allows for conformance to the TG-43 formalism (2) and additionally provides a simplification for the clinical end user regarding the value that must be entered into the treatment planning system. Ultimately, the active length used in the TG-43 dosimetry formalism is intended to serve as an approximate model of the spatial distribution of radioactivity in a source to facilitate accurate data set reproduction and interpolation (2, 6).

### Source strength

Three CS10 sources were calibrated by the National Institute of Standards and Technology (NIST) with the Wide-Angle Free-Air Chamber (WAFAC). The WAFAC provides a primary measurement of air kerma strength,  $S_K$ , for low-energy photon-emitting brachytherapy sources and serves as the national primary standard for this quantity (7). The same three CS10 sources calibrated by NIST were also measured at the UWMRRC with the Variable-Aperture Free-Air Chamber (VAFAC) (8). The VAFAC also provides primary measurements of the  $S_K$  of low-energy photon-emitting brachytherapy sources (7).

During VAFAC measurements, each CS10 source was held vertically in a Kapton tube and rotated at a rate of three rotations-per-minute to average over all azimuthal angles. Each CS10 source was measured three times in one orientation and then flipped  $180^\circ$  along its long axis and measured three more times in the new orientation. MC simulations with the CS10 source model in the VAFAC geometry were used to calculate a correction factor to account for photon attenuation and scatter in the Kapton tube source holder. Simulations were run both with and without the Kapton tube surrounding the CS10 source. An F6 tally was used to score the collision kerma in the VAFAC collecting volume in both simulations. The ratio of the collision kerma without the Kapton tube to the collision kerma with the Kapton tube yielded a correction factor of 1.004. This correction factor was applied to all  $S_K$  measurements. VAFAC correction factors for a 1 cm line source of  $^{103}\text{Pd}$  were obtained from Table 3 of the study by Paxton *et al.* (9) and were applied to the measurements to calculate the quantity  $S_K$ .

The NIST WAFAC  $S_K$  and reproducibility were obtained from the NIST calibration report for the three CS10

sources. The UWMRRC VAFAC  $S_K$  for each CS10 source was calculated as the average of all six VAFAC  $S_K$  measurements. The repeatability of VAFAC  $S_K$  measurements was determined as the standard deviation of the mean of the measured  $S_K$  values using the technique of Culberson *et al.* (8). The VAFAC  $S_K$  values were decay corrected to the WAFAC  $S_K$  measurement reference dates before comparison of the results. Although there are no titanium  $K$ -edge x-rays produced in the CS10 source, the VAFAC aluminum filter was kept in place to be consistent with WAFAC measurements.

#### Azimuthal anisotropy

The internal geometry of the CS10 source is azimuthally asymmetric because of the trapezoidal shape of the  $^{103}\text{Pd}$  regions. To quantify the effect of this asymmetry and verify compatibility with TG-43 dosimetry parameters that assume azimuthal symmetry, the in-air azimuthal anisotropy of the CS10 source was measured with a Ludlum Model 44-3 NaI scintillation detector (Ludlum Measurements, Inc., Sweetwater, TX) and calculated with MC simulations. During NaI scintillation detector measurements, the CS10 source was held vertically in the same Kapton tube that was used for  $S_K$  measurements. The entrance window (diameter of 2.5 cm) of the NaI detector was positioned at a distance of approximately 95 cm from the source along its transverse axis. The source was rotated  $360^\circ$  in steps of  $1.8^\circ$  in the azimuthal direction, with a 300 s counting measurement performed at each azimuthal orientation. The average count rate for each azimuthal orientation was determined as the total counts at that orientation divided by 300 s. This yielded 200 discrete angular measurements for each source. Measured count rates for each source were corrected for source decay and then normalized to the mean value of all 200 measurements for comparison.

The in-air azimuthal anisotropy of the CS10 source was calculated using MC simulations with the CS10 source

model in air. The collision kerma to air in air was scored in a cylindrical shell with a radius of 95 cm, a thickness of 0.002 cm, and a height of 2.5 cm. This cylindrical shell was concentric with the source long axis and was split into 200 angular subdivisions to mimic the angular resolution of the NaI scintillation detector measurements. The notation of Rivard *et al.* (10) was adopted for the azimuthal angle, denoted by  $\psi$ . The azimuthal orientation of the MC model of the CS10 source is indicated by  $\psi$  in Fig. 1. Collision kerma was scored through the use of a \*F4 energy fluence tally modified with  $\mu_{en}/\rho$  values for air from NIST (11). The collision kerma results were normalized to the mean value of all 200 collision kerma values.

#### Phantom design

Two polymethyl-methacrylate (PMMA) phantom templates with dimensions of  $30.0 \times 30.0 \times 0.1 \text{ cm}^3$  were designed for holding the CS10 source and TLD microcubes with dimensions of  $0.1 \times 0.1 \times 0.1 \text{ cm}^3$  for measurements of the TG-43 dose-rate constant,  $\dot{A}$ , two-dimensional (2D) anisotropy function,  $F(r, \theta)$ , and line-source radial dose function,  $g_L(r)$ . The polar anisotropy phantom template was designed for measurement of  $\dot{A}$  and  $F(r, \theta)$ . This phantom contained a central slot that accommodated the source, which was surrounded by four concentric rings of square holes with radii of 1.00, 2.00, 3.00, and 4.00 cm. The 1.00 cm radius ring contained 12 square holes at angular spacings of  $30^\circ$ , and the 2.00, 3.00, and 4.00 cm rings each contained 36 square holes at angular spacings of  $10^\circ$ . The locations of the square holes were selected based on recommendations in the TG-43 report (2). A radial distance of 0.5 cm was not used because TLDs positioned at  $\theta = 0^\circ$  would lie directly on the source. A radial distance of 4.00 cm was chosen instead of the recommended radial distance of 5.00 cm to allow for both higher TLD signals and shorter required irradiation times. A top view and side view of the polar anisotropy phantom are shown in Figs. 2a and 3a, respectively.

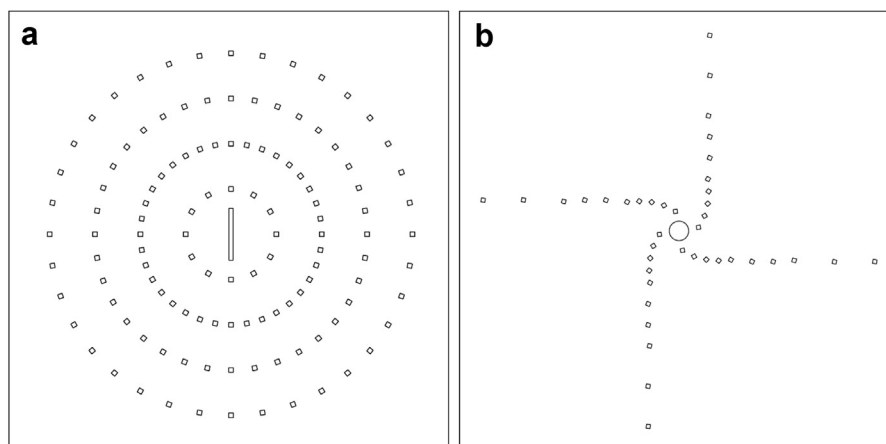


Fig. 2. (a) Diagram of the central region of the polar anisotropy PMMA phantom template. (b) Diagram of the central region of the radial dose PMMA phantom template. Both diagrams are shown to scale. PMMA = polymethyl-methacrylate.

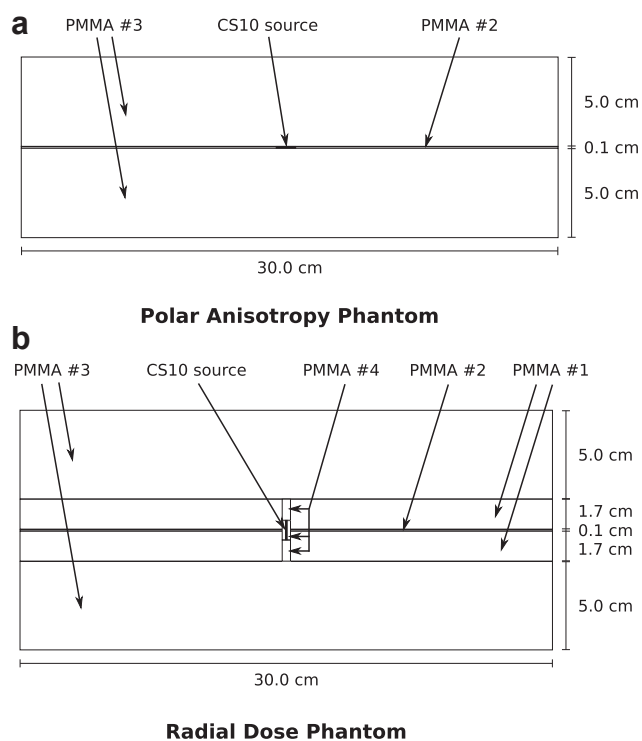


Fig. 3. (a) Side view diagram of the polar anisotropy PMMA phantom geometry. (b) Side view diagram of the radial dose PMMA phantom geometry. Both diagrams are shown to scale. PMMA = polymethyl-methacrylate.

The radial dose phantom template was designed for measurement of  $A$  and  $g_L(r)$ . The source was held within a cylindrical three-piece central source holder plug that extends through the radial dose phantom template. The source was held within the central cylindrical piece of the plug. The source holder plug was surrounded by four spiral “arms” of square holes. Each spiral arm contained 10 square holes at radial distances of 0.50, 0.75, 1.00, 1.25, 1.50, 2.00, 2.50, 3.00, 4.00, and 5.00 cm. The use of square holes allowed for a known orientation of the square-shaped TLD microcubes after placement within the phantom. The positions of these holes relative to the source were selected based on recommendations in the TG-43 report (2). The spiral configuration of the square holes allowed for a direct line-of-sight between the source and each TLD microcube, without interference of holes for other microcubes. A top

view and side view of the radial dose phantom are shown in Figs. 2b and 3b, respectively.

Both the polar anisotropy and the radial dose phantom templates were designed in SolidWorks (Dassault Systèmes SolidWorks Corporation, Waltham, MA), and the designs were sent to Laserage Technology Corporation (Waukegan, IL) for precision laser cutting. During TLD irradiations, additional PMMA phantoms were placed above and below the polar anisotropy phantom template and the radial dose phantom template to provide at least 5 cm of backscattering material beyond all TLD measurement positions as recommended in the TG-43 report (2). The configuration of the polar anisotropy phantom and radial dose phantom geometries are shown in Fig. 3. The PMMA materials used in these phantoms were from four batches of PMMA. Samples from each of the four batches of PMMA were sent to ALS Environmental (Houston, TX) for compositional analyses. The results of these compositional analyses are shown in Table 1 along with the nominal composition for PMMA from NIST (12). The density of the PMMA material was determined from the measured mass and volume of one of the PMMA #1 phantoms (shown in Fig. 3b). The mass was measured with a calibrated American Scientific Products TL2500 scale (American Scientific, LLC, Columbus, OH), and the volume was measured with digital calipers and a ruler. The measured mass and volume yielded a density of  $1.18 \text{ g/cm}^3$  for the PMMA #1 phantom material with an estimated measurement uncertainty of 0.3%. The densities of the PMMA #1, PMMA #2, PMMA #3, and PMMA #4 materials were assumed to be equal.

#### TLD methodology

TLD-100 microcubes placed in the PMMA phantom geometries were used to measure the dose rates at various locations around the CS10 source. These measured dose rates were then used to determine the TG-43 dosimetry parameters for the CS10 source. TLDs were annealed according to a standard regimen used at the UWMRRC. A single annealing cycle involved the transfer of the TLDs to an aluminum tray, a 1-h anneal at  $400^\circ\text{C}$ , a 30-min cool to room temperature on an aluminum block, a 24-h anneal at  $80^\circ\text{C}$ , and finally a 30-min cool to room temperature on an aluminum block. TLDs were irradiated no sooner

Table 1  
Nominal NIST composition of PMMA and measured compositions of the PMMA phantom materials

Element	PMMA (NIST)	PMMA #1	PMMA #2	PMMA #3	PMMA #4
	Weight fraction				
H	0.080538	0.080004	0.080804	0.081534	0.081601
C	0.599848	0.610322	0.614461	0.612091	0.607465
N	—	0.000406	—	0.000253	—
O	0.319614	0.305313	0.304022	0.303892	0.309818
Si	—	0.002231	0.000713	0.002230	0.001116
Ca	—	0.001724	—	—	—

NIST = National Institute of Standards and Technology; PMMA = polymethyl-methacrylate.

than 24 h after completion of an annealing cycle. TLDs were read using a Harshaw 5500 automated reader (Thermo Fisher Scientific, Inc., Waltham, MA). The reading cycle for an individual TLD consisted of a preheat to 50°C, an increase from 50°C to 350°C at a rate of 15 °C/s, and then a hold at 350°C for 26.7 s. TLD light output was measured after the preheat phase to completion of the hold at 350°C. TLDs were corrected for their individual sensitivities based on the magnitude of their light output relative to the median light output of the set of TLDs after an irradiation to a known air kerma level with a <sup>60</sup>Co teletherapy source at the UWMRRC. Additional details about the TLD methodology at the UWMRRC are provided by Nunn *et al.* (13).

Three CS10 sources were individually measured with TLD microcubes in both the polar anisotropy phantom and the radial dose phantom. TLD irradiation times varied depending on the distance of the TLDs from the source. TLDs positioned closer to the source were irradiated for time periods ranging from several hours to several days. TLDs positioned farther from the source were irradiated for time periods ranging from several days to several weeks. The use of different TLD irradiation times allowed for relatively similar doses to be delivered to all TLDs in the phantom, minimizing linearity corrections and the dose range over which the TLDs had to be calibrated. TLDs were calibrated in terms of absorbed dose-to-water with a <sup>60</sup>Co teletherapy source to dose levels ranging from 1 to 200 cGy to bracket the range of doses delivered to the TLDs during the in-phantom irradiations. All TLD holes in the phantoms were always filled with a TLD during the irradiations. The dose rate in water per  $S_K$  for the CS10 source was determined from the TLD measurements using the following equation:

$$\frac{\dot{D}(r, \theta)}{S_K} = \frac{M_{TLD} \cdot N \cdot \lambda \cdot (k_{bq})_{^{60}\text{Co}}^{^{103}\text{Pd}}}{S_K \cdot C(r, \theta) \cdot (e^{-\lambda t_1} - e^{-\lambda t_2})}, \quad (1)$$

where  $\dot{D}(r, \theta)$  is the dose rate in water from the CS10 source at a given radial distance and polar angle,  $S_K$  is the CS10 source air kerma strength (units of  $\mu\text{Gy m}^2 \text{h}^{-1}$ ) at the start time for the TLD irradiation,  $M_{TLD}$  is the fully corrected TLD light output (in nC),  $N$  is the average <sup>60</sup>Co calibration coefficient (in cGy/nC) based on the readings of 30 TLDs,  $\lambda$  is the decay constant for <sup>103</sup>Pd,  $(k_{bq})_{^{60}\text{Co}}^{^{103}\text{Pd}}$  is the ratio of the intrinsic energy dependence (14) for <sup>103</sup>Pd and <sup>60</sup>Co,  $C(r, \theta)$  is an MC-calculated correction factor that accounts for the absorbed dose energy dependence (14) from <sup>103</sup>Pd to <sup>60</sup>Co, the finite size of the TLDs, attenuation and scatter within the TLDs, and conversion from dose-to-TLD in a PMMA medium to dose-to-water in a water medium, and  $t_1$  and  $t_2$  are the start and end times of the TLD irradiation, respectively.

The intrinsic energy dependence,  $k_{bq}(Q)$ , was used according to the definition provided by DeWerd *et al.* (14), given by

$$k_{bq}(Q) = \frac{D_{TLD}(Q)}{M_{TLD}(Q)}, \quad (2)$$

where  $Q$  is the photon beam quality,  $D_{TLD}$  is the dose to the TLD, and  $M_{TLD}$  is the TLD light output. The ratio of  $k_{bq}(^{103}\text{Pd})$  to  $k_{bq}(^{60}\text{Co})$ , denoted as  $(k_{bq})_{^{60}\text{Co}}^{^{103}\text{Pd}}$ , was used to account for the change in TLD intrinsic energy dependence from <sup>103</sup>Pd photon energies to <sup>60</sup>Co photon energies.  $(k_{bq})_{^{60}\text{Co}}^{^{103}\text{Pd}}$  was calculated as the inverse of the  $\eta(X)$  value interpolated between the M40 and M50 x-ray beam qualities in Table 2 of the study by Nunn *et al.* (13) for an energy of 21.2 keV, yielding a value of 0.913. The 21.2 keV energy used for interpolation is the weighted mean energy of the CS10 source photon spectrum at the TG-43 reference position ( $r = 1 \text{ cm}$ ,  $\theta = 90^\circ$ ) in a PMMA medium as calculated using MC simulations with an F2 surface flux tally.

### MC methodology

The CS10 source was modeled in the MCNP5 v1.60 MC radiation transport code (15) with the mcplib84 photon cross-section data library. Each <sup>103</sup>Pd region was modeled as having 8.3  $\mu\text{g}$  of Pd distributed uniformly throughout the organic polymer. The variability ( $k = 1$ ) of loading <sup>103</sup>Pd into each well in the same batch is about 1% as measured at CivaTech Oncology, Inc. The variability ( $k = 1$ ) of  $S_K$  in a batch of five CS10 sources was about 1.5% as measured at NIST. The <sup>103</sup>Pd photon spectrum from the National Nuclear Data Center online NUDAT 2.6 database (16) was used for all MC simulations with the CS10 source.

MC simulations were used to calculate the  $C(r, \theta)$  correction factor used in Eq. 1 and to calculate the TG-43 dosimetry parameters for the CS10 source. Collision kerma was used as an approximation for the absorbed dose (2) in all CS10 MC simulations. Six simulation geometries were

Table 2  
Uncertainty analysis for the TLD measurements of the CS10 A

Parameter	Type A (%)	Type B (%)
TLD reproducibility	0.57	
TLD positioning		1.50
Source positioning		0.12
<sup>60</sup> Co air kerma rate		0.73
Source air kerma strength		0.83
TLD calibration		1.91
PMMA density and composition		0.62
$\mu/\rho$ values		1.39
$\mu_{en}/\rho$ values		1.23
TLD intrinsic energy dependence correction		2.29
Quadratic sum	0.57	4.02
Combined standard uncertainty ( $k = 1$ )		4.06
Expanded uncertainty ( $k = 2$ )		8.13

TLD = thermoluminescent dosimeter; PMMA = polymethylmethacrylate.

required for these calculations, with at least 10 billion histories used in each simulation:

1. CS10 source and TLDs in the polar anisotropy PMMA phantom
2. CS10 source and TLDs in the radial dose PMMA phantom
3. CS10 source in a water medium
4. CS10 source *in vacuo*
5. Water disk in a water cube in the  $^{60}\text{Co}$  irradiation geometry
6. TLD disk in a water cube in the  $^{60}\text{Co}$  irradiation geometry

Geometries 1 and 2 consisted of the CS10 source and TLD microcubes positioned in the polar anisotropy PMMA phantom setup and radial dose PMMA phantom setup, respectively, as shown in Figs. 2 and 3. All square holes were filled with a TLD microcube. The PMMA densities were set to  $1.18 \text{ g/cm}^3$ , and the PMMA compositions were set to match the measured compositions shown in Table 1. Simulations for these geometries were run with photon transport alone with a 1 keV photon energy cutoff. A \*F4 energy fluence tally modified with  $\mu_{\text{en}}/\rho$  values for LiF from NIST (11) was used to score the dose-to-TLD in the individual TLDs.

Geometry 3 consisted of the CS10 source positioned in the center of a water sphere with a radius of 15 cm. The source was surrounded by rings of water placed at distances and polar angles that corresponded to the distances and polar angles of the TLDs in the polar anisotropy and radial dose PMMA phantoms. All rings subtended a  $\pm 0.5^\circ$  polar angle region around the source for each angle of interest. Simulations with this geometry were run with photon transport alone with a 1 keV photon energy cutoff. A \*F4 energy fluence tally modified with  $\mu_{\text{en}}/\rho$  values for water from NIST (11) was used to score the dose-to-water in each ring of water.

Geometry 4 consisted of the CS10 source positioned *in vacuo*. An air ring with a radius of 30 cm and a thickness of 0.0002 cm was positioned concentric with the source long axis. The air ring subtended an angle of  $\pm 7.6^\circ$  with respect to the source transverse axis to mimic the WAFAC collecting region for  $S_K$  measurements. The simulation was run with photon transport alone. A 5-keV photon energy cutoff was selected to comply with the lower energy cutoff in the definition of  $S_K$  (2). A \*F4 energy fluence tally modified with  $\mu_{\text{en}}/\rho$  values for air from NIST (11) was used to score the air kerma in the air rings.

Geometries 5 and 6 each consisted of a  $30 \text{ cm} \times 30 \text{ cm} \times 30 \text{ cm}$  water cube positioned with its front face at a distance of 95 cm from a  $^{60}\text{Co}$  point source. The  $^{60}\text{Co}$  photon spectrum was determined from a separate simulation of the UWMRRC  $^{60}\text{Co}$  irradiator in which an energy-binned F5 tally was used to score the fluence at a distance of 95 cm from the source in air. The water cube geometry was used to determine the ratio of the dose-to-water to the dose-to-TLD for  $^{60}\text{Co}$  photon energies. Each simulation geometry

consisted of a disk with a thickness of 0.01 cm and a radius of 0.5 cm placed at a distance of 100 cm from the source at a 5 cm depth in the water tank. Geometry 5 contained a disk filled with water, and Geometry 6 contained a disk filled with TLD material. These simulations were run with coupled photon and electron transport with 1 and 10 keV cutoffs for photons and electrons, respectively. A \*F8 energy deposition tally was used to score the energy deposited in the water disk and in the TLD disk. The calculated energy deposition in the water disk and in the TLD disk was converted to the quantity absorbed dose via division by their associated masses.

MC simulation results for Geometries 1–6 were used to calculate the  $C(r, \theta)$  correction factor, given by the following equation:

$$C(r, \theta) = \left( \frac{D_{\text{TLD}}(r, \theta)}{D_{\text{water}}(r, \theta)} \right)_{^{103}\text{Pd}} \cdot \left( \frac{D_{\text{water}}}{D_{\text{TLD}}} \right)_{^{60}\text{Co}}, \quad (3)$$

where  $D_{\text{TLD}}(r, \theta)$  for  $^{103}\text{Pd}$  is the dose-to-TLD from the CS10 source at a given position in the PMMA phantom geometry (determined from the Geometries 1 and 2 simulations),  $D_{\text{water}}(r, \theta)$  for  $^{103}\text{Pd}$  is the dose-to-water from the CS10 source at a given position in a water medium (determined from the Geometry 3 simulation), and the ratio of  $D_{\text{water}}$  to  $D_{\text{TLD}}$  for  $^{60}\text{Co}$  is the dose-to-water per dose-to-TLD in the  $^{60}\text{Co}$  irradiation geometry (determined from the Geometry 5 and Geometry 6 simulations).

$A$  was calculated as the dose-to-water at a distance of 1 cm along the transverse axis of the source in a water medium (determined from the Geometry 3 simulation) divided by the product of the air kerma in the air ring at 30 cm from the source (determined from the Geometry 4 simulation) and the square of the distance between the source and the air ring.  $A$  was calculated for a WAFAC-like integration region.  $F(r, \theta)$  and  $g_L(r)$  were calculated from the Geometry 3 simulation.

#### Uncertainty analysis

Uncertainty analyses were completed for the TLD measurements of the CS10  $A$ ,  $F(r, \theta)$ , and  $g_L(r)$  and for MC calculations of the CS10  $A$  in accordance with the methodologies set forth in the American Association of Physicists in Medicine Task Group No. 138 report by DeWerd *et al.* (17) and the NIST Technical Note 1297 (18).

Uncertainties associated with TLD measurements of  $A$  are shown in Table 2 and were determined as follows:

- The TLD reproducibility was estimated from the standard deviation of the mean for 72 individual measurements of  $A$ .
- Uncertainty due to TLD positioning in the PMMA phantoms was estimated from MC simulations with TLD microcubes positioned at a radial distance of both 1.00 and 0.98 cm to determine the effect of a 0.02 cm shift in position.

- Source positioning uncertainty was estimated from MC simulations with the CS10 source centered in the radial dose phantom and with the CS10 source shifted by 0.05 cm along its long axis.
- The  $^{60}\text{Co}$  air kerma rate uncertainty was estimated from ionization chamber measurements at the University of Wisconsin Accredited Dosimetry Calibration Laboratory.
- Source air kerma strength uncertainty was estimated from the average of the combined standard uncertainties ( $k = 1$ ) for the NIST WAFAC measurements of the three CS10 sources, which were calculated from the Type A (reproducibility) and estimated Type B uncertainties.
- TLD calibration uncertainty was estimated from the percentage differences between the actual doses delivered to the calibration TLDs and the doses determined from application of an average calibration coefficient to the calibration TLD light output values.
- Uncertainty due to PMMA density and composition was estimated from the percentage difference between MC simulations of the dose-to-TLD at the TG-43 reference position in the radial dose PMMA phantom with the NIST density ( $1.19 \text{ g/cm}^3$ ) (12) and composition and with the measured density ( $1.18 \text{ g/cm}^3$ ) and composition. PMMA compositions are shown in Table 1.
- Uncertainty in the  $\mu_{\text{en}}/\rho$  values for water was based on the estimated standard uncertainties of 0.91% and 0.82% for 17.5 and 24.6 keV photon energies, respectively, from the study by Andreo *et al.* (19). The weighted mean energy of  $^{103}\text{Pd}$  *in vacuo* is 20.74 keV (2), and this energy was used to interpolate between the two uncertainty values reported by Andreo *et al.* (19), yielding an uncertainty of 0.87% for  $^{103}\text{Pd}$ . The uncertainty in the  $\mu_{\text{en}}/\rho$  values for LiF was estimated to be equivalent to that of water. The uncertainties for water and LiF were added in quadrature to estimate the overall uncertainty due to the  $\mu_{\text{en}}/\rho$  values.
- Uncertainty in the  $\mu/\rho$  values for water was assigned a value of 0.80% based on the estimates of Hubbell (20) that uncertainties in  $\mu_{\text{en}}/\rho$  are slightly greater than those for  $\mu/\rho$ . Uncertainty in the  $\mu/\rho$  values for PMMA and LiF was estimated to be equivalent to that of water. The  $\mu/\rho$  uncertainties for water, PMMA, and LiF were added in quadrature to estimate the overall uncertainty due to the  $\mu/\rho$  values.
- Uncertainty in the TLD intrinsic energy dependence correction was obtained from Table 2 of the study by Nunn *et al.* (13).

Uncertainties associated with TLD measurements of  $F(r, \theta)$  were estimated based on the standard deviation of the mean of the TLD measurements, the inverse square effect of a 0.01 cm change in the source-to-TLD distance, and the effect of using the measured PMMA density and composition vs. the NIST PMMA density and composition

in the MC simulations. These uncertainties were combined in quadrature and are shown at the  $k = 2$  level in Table 5. Uncertainties associated with TLD measurements of  $g_L(r)$  were estimated using the same approach as that for  $F(r, \theta)$  with the addition of an assigned 1% uncertainty in the TLD calibration to account for the variation in the magnitude of the dose delivered to the TLDs positioned at various radial distances. These uncertainties were combined in quadrature and are shown at the  $k = 2$  level in Table 7.

Uncertainties associated with MC calculations of  $\mathcal{A}$  are shown in Table 3 and were determined as follows:

- Uncertainty due to tally statistics is based on the standard deviation of the mean for the MC simulation results.
- Uncertainty due to source positioning was estimated in the same manner as was used in the TLD uncertainty analysis.
- Uncertainty due to the  $^{103}\text{Pd}$  photon spectrum was estimated from the percentage differences in the MC simulation results for the dose-to-water at the TG-43 reference position in Geometry 3 and the air kerma in Geometry 4 when using the  $^{103}\text{Pd}$  photon spectrum from the TG-43 report (2) vs. the  $^{103}\text{Pd}$  photon spectrum from the National Nuclear Data Center online NUDAT 2.6 database (16).
- Uncertainty in the  $\mu_{\text{en}}/\rho$  values for water was estimated in the same manner as was used in the TLD uncertainty analysis. The uncertainty in the  $\mu_{\text{en}}/\rho$  values for air for  $^{103}\text{Pd}$  was determined via interpolation between the estimated standard uncertainties of 0.84% and 0.76% for 17.5 and 24.6 keV photon energies, respectively, from the study by Andreo *et al.* (19). The uncertainties for water and air were added in quadrature to estimate the overall uncertainty due to the  $\mu_{\text{en}}/\rho$  values.
- Uncertainty in  $\mu/\rho$  values for water was estimated in the same manner as was used in the TLD analysis.

## Results

### Source strength

The  $S_K$  values for the three CS10 sources as measured with the WAFAC (NIST) and the VAFAC (UWMRRC)

Table 3  
Uncertainty analysis for the MC calculations of the CS10  $\mathcal{A}$

Parameter	Type A (%)	Type B (%)
Tally statistics	0.02	
Source positioning		0.12
Photon spectrum		0.05
$\mu/\rho$ values		0.80
$\mu_{\text{en}}/\rho$ values		1.18
Quadratic sum	0.02	1.43
Combined standard uncertainty ( $k = 1$ )		1.43
Expanded uncertainty ( $k = 2$ )		2.87

MC = Monte Carlo.

Table 4

 $S_K$  measurements of three CS10 sources with the WAFAC (NIST) and the VAFAC (UWMRRC)

UWMRRC Source number	NIST measurements		UWMRRC measurements		% Difference, VAFAC vs. WAFAC
	WAFAC $S_K$ ( $\mu\text{Gy}\cdot\text{m}^2\cdot\text{h}^{-1}$ )	Reproducibility (%)	VAFAC $S_K$ ( $\mu\text{Gy}\cdot\text{m}^2\cdot\text{h}^{-1}$ )	Repeatability (%)	
CS10-1	4.15	0.46	4.18	0.57	0.6
CS10-2	4.58	0.37	4.58	0.34	0.0
CS10-3	4.11	0.33	4.15	1.1	0.9

WAFAC = Wide-Angle Free-Air Chamber; NIST = National Institute of Standards and Technology; VAFAC = Variable-Aperture Free-Air Chamber; UWMRRC = University of Wisconsin Medical Radiation Research Center.

are shown in Table 4. The VAFAC  $S_K$  results agree to within 1% of the WAFAC  $S_K$  results. The reproducibility and repeatability for the  $S_K$  measurements account for the statistical variations in the free-air ionization chamber current measurements and the variation that stems from measurements of the source in two opposite orientations along the long axis. The maximum difference in CS10 VAFAC  $S_K$  measurements between opposite orientations along the source long axis was 0.4%.

#### Azimuthal anisotropy

The measured in-air azimuthal anisotropy of the three CS10 sources and the MC-calculated results are shown in Fig. 4. The measured results for each source and the MC results were normalized to their respective means. The azimuthal orientation of each source at the beginning of the measurement was random, so a given azimuthal angle in Fig. 4 does not necessarily correspond to the same physical source orientation across all three sources. The in-air azimuthal anisotropy data show a high degree of azimuthal symmetry, with  $\geq 95\%$  of the normalized values for each source lying within 1.2% of the mean value.

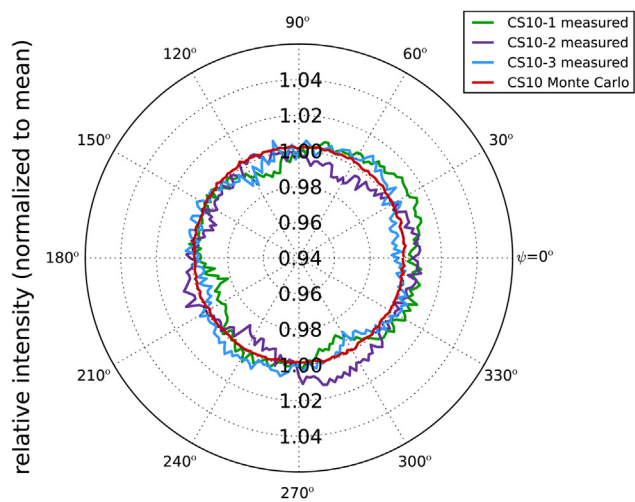


Fig. 4. In-air azimuthal anisotropy of three CS10 sources as measured with a NaI scintillation detector and as calculated with MC simulations. Absolute values of the azimuthal angle  $\psi$  are only relevant for the MC data because the source azimuthal orientation was unknown during measurements. MC = Monte Carlo.

#### Dose-rate constant

TLD measurements of the CS10 A yielded a value of  $0.660 \pm 0.054$  cGy/h/U ( $k = 2$ ). MC calculations of the CS10 A yielded a value of  $0.622 \pm 0.018$  cGy/h/U ( $k = 2$ ). The A values determined from TLD measurements and from MC calculations agree to within the TLD

Table 5

CS10  $F(r, \theta)$  determined with TLD measurements and MC simulations

Radial distance (cm)	Polar angle ( $^\circ$ )	TLD, $F(r, \theta)$ , $L = 1.0$ cm (%)	MC, $F(r, \theta)$ , $L = 1.0$ cm	Ratio (TLD/MC)
1.00	0	$0.915 \pm 0.073$ (8.0)	0.962	0.95
1.00	30	$1.096 \pm 0.062$ (5.7)	1.113	0.98
1.00	60	$1.025 \pm 0.049$ (4.8)	1.034	0.99
1.00	90	$1.000 \pm 0.049$ (4.9)	1.000	1.00
2.00	0	$0.853 \pm 0.034$ (4.0)	0.876	0.97
2.00	10	$1.032 \pm 0.042$ (4.0)	1.052	0.98
2.00	20	$1.045 \pm 0.035$ (3.3)	1.067	0.98
2.00	30	$1.060 \pm 0.034$ (3.2)	1.063	1.00
2.00	40	$1.057 \pm 0.029$ (2.7)	1.051	1.01
2.00	50	$1.039 \pm 0.031$ (3.0)	1.035	1.00
2.00	60	$1.026 \pm 0.028$ (2.7)	1.021	1.01
2.00	70	$1.024 \pm 0.025$ (2.5)	1.010	1.01
2.00	80	$1.022 \pm 0.026$ (2.6)	1.003	1.02
2.00	90	$1.000 \pm 0.025$ (2.5)	1.000	1.00
3.00	0	$0.851 \pm 0.033$ (3.9)	0.864	0.98
3.00	10	$1.006 \pm 0.027$ (2.6)	1.030	0.98
3.00	20	$1.019 \pm 0.030$ (2.9)	1.047	0.97
3.00	30	$1.033 \pm 0.027$ (2.6)	1.046	0.99
3.00	40	$1.040 \pm 0.027$ (2.6)	1.038	1.00
3.00	50	$1.023 \pm 0.027$ (2.7)	1.027	1.00
3.00	60	$0.998 \pm 0.034$ (3.5)	1.016	0.98
3.00	70	$1.014 \pm 0.036$ (3.6)	1.008	1.01
3.00	80	$1.012 \pm 0.025$ (2.4)	1.003	1.01
3.00	90	$1.000 \pm 0.027$ (2.7)	1.000	1.00
4.00	0	$0.893 \pm 0.036$ (4.0)	0.870	1.03
4.00	10	$1.036 \pm 0.037$ (3.5)	1.018	1.02
4.00	20	$1.047 \pm 0.039$ (3.7)	1.036	1.01
4.00	30	$1.047 \pm 0.041$ (4.0)	1.036	1.01
4.00	40	$1.043 \pm 0.040$ (3.9)	1.031	1.01
4.00	50	$1.045 \pm 0.039$ (3.8)	1.022	1.02
4.00	60	$1.002 \pm 0.052$ (5.2)	1.014	0.99
4.00	70	$1.014 \pm 0.040$ (4.0)	1.006	1.01
4.00	80	$1.026 \pm 0.037$ (3.6)	1.002	1.02
4.00	90	$1.000 \pm 0.045$ (4.5)	1.000	1.00

TLD = thermoluminescent dosimeter; MC = Monte Carlo.

Note. Estimated absolute TLD uncertainties at the  $k = 2$  level are included, with percentage uncertainties shown in parenthesis.

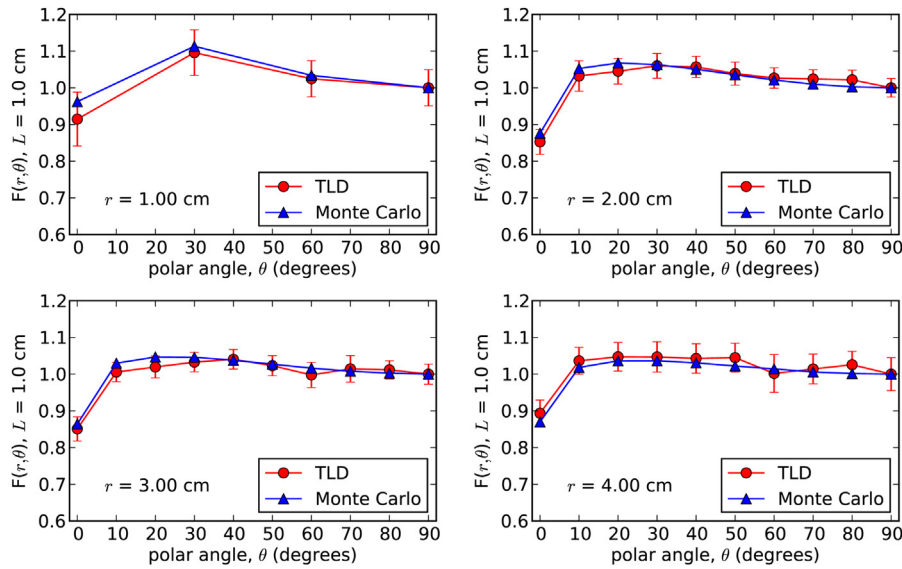


Fig. 5. CS10  $F(r, \theta)$  determined with TLD measurements and MC simulations at four different radii. TLD = thermoluminescent dosimeter; MC = Monte Carlo.

uncertainties ( $k = 2$ ). The equally weighted average of the TLD and MC  $\Lambda$  values is 0.641 cGy/h/U, which is approximately 6.5% lower than the TG-43 consensus  $\Lambda$  values for both the TheraSeed model 200 (Theragenics Corp., Buford, GA) (2) and the Best model 2335 (Best Medical International, Springfield, VA) (21).

*Polar anisotropy*

The  $F(r, \theta)$  results are shown in Table 5 and Fig. 5. TLD and MC results for radial distances of 1, 2, 3, and 4 cm agree to within the TLD uncertainties ( $k = 2$ ) as indicated by the absolute uncertainties shown in Table 5. For all radii, the TLD and MC  $F(r, \theta)$  values are within 15% of unity. When excluding data for  $r = 1$  cm and for  $\theta = 0^\circ$ , all values are within 7% of unity. The CS10  $F(r, \theta)$  values remain relatively flat over most angles, with a sharp falloff at  $\theta = 0^\circ$ . For  $r = 1, 2, 3,$  and  $4$  cm, the TG-43 consensus  $F(r, \theta)$  values for the model 200 (2) and model 2335 (21) sources are up to 50% and 40% less than unity, respectively, and exhibit considerable angular dependence.

Derived from the  $F(r, \theta)$  values in Table 5, the one-dimensional (1D) anisotropy function values from the TLD and MC results are included in Table 6. These values, in combination with the 1D geometry function, may be used for 1D dose calculations using the TG-43 formalism (2). However, the authors do not suggest this be performed for clinical implants with CivaString sources where the source orientation is known. This is because the 2D dose calculation formalism provides a more accurate representation of the dose distribution around the source (Fig. 6) due to volume averaging as a function of polar angle using the 1D formalism. Here, the ratio of the dose distributions using the 1D and 2D formalisms is depicted, showing dose errors exceeding +84% and -90% can occur within 5 mm of the source when using the 1D formalism. Because of the long active length of the CS10 source, the magnitude and extent of these dose errors when using the 1D formalism is more dramatic than for the typical seed.

*Line-source radial dose function*

$g_L(r)$  results are shown in Table 7 and Fig. 7. TLD and MC results agree to within the TLD uncertainties ( $k = 2$ ) for  $r \leq 2.50$  cm as indicated by the absolute uncertainties shown in Table 7. The TLD results trend higher than the MC results with increasing radial distance, similar to the trends observed by Dolan et al. (4) and Kennedy et al. (22). The differences at greater distances are likely due to increased uncertainties in the TLD measurement correction factors used to convert from dose-to-TLD in a PMMA medium to dose-to-water in a water medium. Compared with the TG-43 consensus  $g_L(r)$  values for the model 200 (2) and model 2335 (21) sources, the CS10 MC  $g_L(r)$  values are consistently lower for  $r < 1$  cm with up to a 6% difference

Table 6  
CS10 1D anisotropy function values derived from the 2D anisotropy function values for TLD measurements and MC simulations

Radial distance (cm)	TLD this study	MC this study	MC Rivard et al. (5)
1.00	1.117	1.125	1.170
2.00	1.056	1.051	1.057
3.00	1.026	1.030	1.031
4.00	1.030	1.021	1.022

1D = one-dimensional; 2D = two-dimensional; TLD = thermoluminescent dosimeter; MC = Monte Carlo. Note. Values from Rivard et al. (5) are also included for comparison.

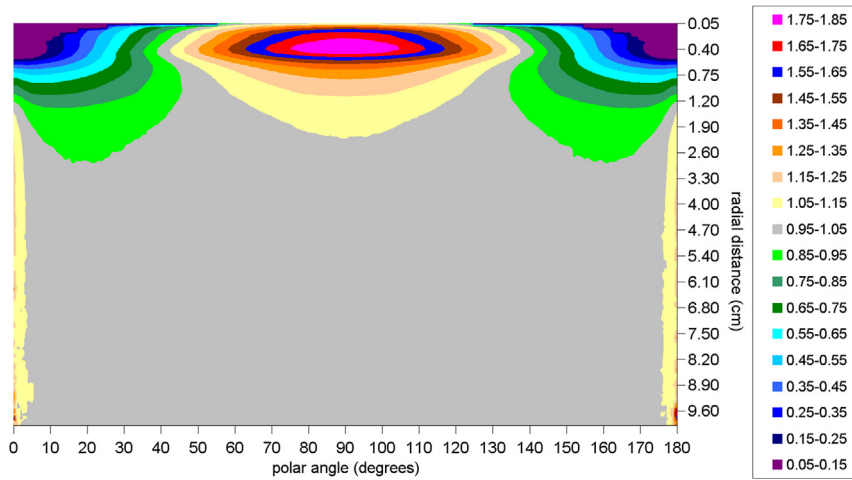


Fig. 6. Ratio of the CS10 dose distributions using the 1D and 2D dose calculation formalisms adapted from Rivard *et al.* (5). 1D = one-dimensional; 2D = two-dimensional.

and are consistently higher for  $r > 1$  cm with up to a 9% difference.

**Discussion**

The results of the in-air azimuthal anisotropy measurements and MC calculations showed that the minimally azimuthally asymmetric internal geometry of the CS10 source resulted in minimal fluctuations in its azimuthal intensity. This indicated that the TG-43 dosimetry parameters that assume azimuthal symmetry can appropriately be used to describe the CS10 dose distribution. TG-43 dosimetry parameters of the CS10 source determined through TLD measurements and MC simulations agree to within the associated uncertainties ( $k = 2$ ).

The CS10 TG-43 dosimetry parameters are noticeably different than those for the model 200 and model 2335 sources. These differences result from the novel design of the CS10 source, which consists of an elongated physical structure, an extended distribution of radioactive material,

and a low-Z organic polymer composition. Differences in  $A$  result from the unique distribution of radioactive material within the CS10 source as compared with the model 200 and model 2335 sources. The radioactive material in the CS10 source is distributed over a length of approximately 1.0 cm, which increases the distance between much of the radioactive material and the TG-43 reference position compared with a source with a more centralized and point-like distribution of radioactive material. This results in a reduced ratio of the CS10 dose rate in water at the TG-43 reference position to the source  $S_K$  as compared with that for the model 200 and model 2335 sources.

Differences in  $F(r, \theta)$  result from the low-Z organic polymer composition of the CS10 source, which results in less perturbation of the dose distribution than sources with a titanium encapsulation and titanium end welds. The CS10 dose distribution is relatively homogeneous for  $r \geq 1$  cm, as shown by the minimal changes in  $F(r, \theta)$  away from  $\theta = 0^\circ$ . The only perturbations in the CS10 dose distribution are the dips at  $\theta = 0^\circ$  that result from the shielding effect of the gold marker in the center of the source.

Table 7  
CS10  $g_L(r)$  determined with TLD measurements and MC simulations

Radial distance (cm)	TLD, $g_L(r)$ , $L = 1.0$ cm (%)	MC, $g_L(r)$ , $L = 1.0$ cm	Ratio (TLD/MC)
0.50	1.210 ± 0.105 (8.7)	1.232	0.98
0.75	1.101 ± 0.067 (6.1)	1.122	0.98
1.00	1.000 ± 0.056 (5.6)	1.000	1.00
1.25	0.893 ± 0.051 (5.7)	0.881	1.01
1.50	0.799 ± 0.046 (5.7)	0.770	1.04
2.00	0.622 ± 0.042 (6.8)	0.580	1.07
2.50	0.473 ± 0.041 (8.7)	0.432	1.10
3.00	0.365 ± 0.036 (10)	0.319	1.14
4.00	0.206 ± 0.029 (14)	0.172	1.19
5.00	0.116 ± 0.021 (18)	0.092	1.26

TLD = thermoluminescent dosimeter; MC = Monte Carlo.

Note. Estimated absolute TLD uncertainties at the  $k = 2$  level are included, with percentage uncertainties shown in parenthesis.

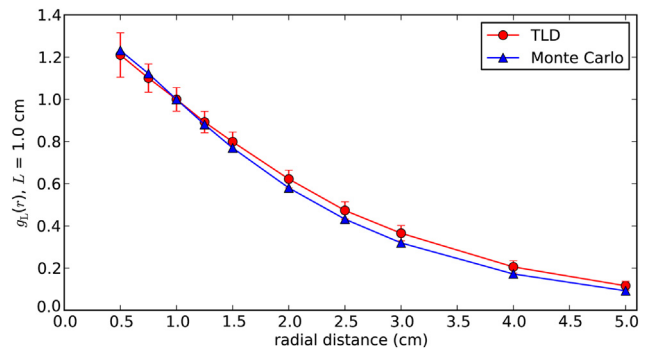


Fig. 7. CS10  $g_L(r)$  determined with TLD measurements and MC simulations. TLD = thermoluminescent dosimeter; MC = Monte Carlo.

Differences in  $g_L(r)$  stem from the same origin as the differences in  $A$ , namely the extended distribution of radioactive material within the CS10. This causes a reduced ratio of the dose rate in water per  $S_K$  at the TG-43 reference position, which is the normalization point for  $g_L(r)$ . This results in higher  $g_L(r)$  values for  $r > 1$  cm. As  $r$  decreases from 1 cm toward the source surface, the distribution of radioactive material appears more and more spread out, causing  $g_L(r)$  to be lower than that for the model 200 and model 2335 that have radioactive material distributed over a shorter linear distance.

## Conclusions

This study provides CS10 source TG-43 dosimetry parameters determined through TLD measurements and MC simulations in accordance with the approach recommended in TG-43 (2). Additionally, differences in the dose distribution for the CS10 source and the model 200 and model 2335 sources are explained in relation to their differing designs. This study demonstrated that the minimally azimuthally asymmetric design of the CivaString CS10 source has a minimal impact on its azimuthal anisotropy and that an assumption of azimuthal symmetry is appropriate. CS10 TG-43 dosimetry parameters were determined through TLD measurements and MC simulations and were shown to agree within the associated uncertainties. The CS10 dose distribution was compared with that for the model 200 and model 2335 sources, indicating that the CS10 dose distribution is more homogeneous because of its low- $Z$  organic polymer composition and stable geometry.

## Acknowledgments

The authors thank CivaTech Oncology for providing the CS10 sources, Dr. Seth Hoedl and Dr. Kristy Perez for their support in this work, and Dr. Michael Mitch for providing Wide-Angle Free-Air Chamber  $S_K$  measurement data and uncertainties for the three CS10 sources measured at the National Institute of Standards and Technology. The authors additionally thank the students and staff of the University of Wisconsin Medical Radiation Research Center, especially Ben Palmer for his assistance with the polymethylmethacrylate phantom design and machining and Cliff Hammer for his assistance with thermoluminescent dosimeter handling and analysis. Finally, the authors thank the customers of the University of Wisconsin Accredited Dosimetry Calibration Laboratory for their financial support of this laboratory through their instrument calibrations.

## References

[1] Yu Y, Anderson LL, Li Z, et al. Permanent prostate seed implant brachytherapy: Report of the American Association of Physicists in Medicine Task Group No. 64. *Med Phys* 1999;26:2054–2076.

- [2] Rivard MJ, Coursey BM, DeWerd LA, et al. Update of AAPM Task Group No. 43 Report: A revised AAPM protocol for brachytherapy dose calculations. *Med Phys* 2004;31:633–674.
- [3] Thomadsen BR, Williamson JR, Rivard MJ, et al. Anniversary paper: Past and current issues, and trends in brachytherapy physics. *Med Phys* 2008;35:4708–4723.
- [4] Dolan J, Li Z, Williamson JR. Monte Carlo and experimental dosimetry of an 125I brachytherapy seed. *Med Phys* 2006;33:4675–4684.
- [5] Rivard MJ, Reed JL, DeWerd LA. 103Pd strings: Monte Carlo assessment of a new approach to brachytherapy source design. *Med Phys* 2014;41:011716.
- [6] Rivard MJ, Coursey BM, DeWerd LA, et al. Comment on “Let’s abandon geometry factors other than that of a point source in brachytherapy dosimetry”. *Med Phys* 2002;29:1919–1920.
- [7] Seltzer SM, Lamperti PJ, Loevinger R, et al. New national air-kerma-strength standards for 125I and 103Pd brachytherapy seeds. *J Res Natl Inst Stand Technol* 2003;108:337–358.
- [8] Culberson WS, DeWerd LA, Anderson DR, et al. Large-volume ionization chamber with variable apertures for air-kerma measurements of low-energy radiation sources. *Rev Sci Instrum* 2006;77:1–9.
- [9] Paxton AB, Culberson WS, DeWerd LA, et al. Primary calibration of coiled 103Pd brachytherapy sources. *Med Phys* 2008;35:32–38.
- [10] Rivard MJ, Melhus CS, Kirk BL. Brachytherapy dosimetry parameters calculated for a new 103Pd source. *Med Phys* 2004;31:2466–2470.
- [11] Tables of x-ray mass attenuation coefficients and mass energy-absorption coefficients from 1 keV to 20 MeV for elements  $Z = 1$  to 92 and 48 additional substances of dosimetric interest, National Institute of Standards and Technology. Available at: <http://www.nist.gov/pml/data/xraycoef/index.cfm>. Accessed January 14, 2014.
- [12] Compositions of materials used in STAR databases, National Institute of Standards and Technology. Available at: <http://physics.nist.gov/cgi-bin/Star/compos.pl>. Accessed January 14, 2014.
- [13] Nunn AA, Davis SD, Micka JA, et al. LiF: Mg,Ti TLD response as a function of photon energy for moderately filtered x-ray spectra in the range of 20–250 kVp relative to 60Co. *Med Phys* 2008;35:1859–1869.
- [14] DeWerd LA, Bartol LJ, Davis SD. Thermoluminescence dosimetry. Proceedings of the AAPM Summer School 2009;34:815–840.
- [15] Brown F, Kiedrowski B, Bull J. *MCNP5 1.60 release notes. Report No. LA-UR-10-06235*. Los Alamos, NM: Los Alamos National Laboratory; 2010.
- [16] NUDAT 2.6, National Nuclear Data Center, Brookhaven National Laboratory. Available at: <http://www.nndc.bnl.gov/nudat2/>. Accessed January 14, 2014.
- [17] DeWerd LA, Ibbott GS, Meigooni AS, et al. A dosimetric uncertainty analysis for photon-emitting brachytherapy sources: Report of AAPM Task Group No. 138 and GEC-ESTRO. *Med Phys* 2011;38:782–801.
- [18] Taylor BN, Kuyatt CE. *NIST Technical Note 1297: guidelines for evaluating and expressing the uncertainty of NIST measurement results*. Gaithersburg, MD: Technical Report, National Institute of Standards and Technology; 1994.
- [19] Andreo P, Burns DT, Salvat F. On the uncertainties of photon mass energy-absorption coefficients and their ratios for radiation dosimetry. *Phys Med Biol* 2012;57:2117–2136.
- [20] Hubbell JH. Photon mass attenuation and energy-absorption coefficients from 1 keV to 20 MeV. *Int J Appl Radiat Isot* 1982;33:1269–1290.
- [21] Rivard MJ, Butler WM, DeWerd LA, et al. Supplement to the 2004 update of the AAPM Task Group No. 43 Report. *Med Phys* 2007;34:2187–2205.
- [22] Kennedy RM, Davis SD, Micka JA, et al. Experimental and Monte Carlo determination of the TG-43 dosimetric parameters for the model 9011 THINSeedTM brachytherapy source. *Med Phys* 2010;37:1681–1688.